The characteristics and kinetics of co-pyrolysis of furfural residue with oil shale semi-coke

Yu Yang[a]*, Ye Chen[b], Yuchuan Deng[a], Xuanyu Ji[a]

[a] College of Mechanical and Power Engineering, Chongqing University of Science & Technology, Chongqing 401331, China
[b] Sichuan Provincial Key Lab of Process Equipment and Control, Zigong 643000, China

Abstract. *In the present work, the thermogravimetric analysis-Fourier transform infared spectroscopy (TGA-FTIR) system was employed to investigate the co-pyrolysis behavior of oil shale (OS) semi-coke (SC) and furfural residue (FR). Results indicated that the addition of furfural residue improved the pyrolysis characteristics of blends, while synergy behaved differently with the variation of the mixing proportion. Semi-coke could act as a catalyst for the furfural residue pyrolysis and facilitated the release of hydroxyl, but slightly inhibited the release of CO_2 and CH_4. The optimal blending ratio of oil shale semi-coke to furfural residue was 1:1. Besides, kinetic parameters were calculated using model-free methods, declaring that the sample pyrolysis was a multi-process.*

Keywords: *oil shale semi-coke, furfural residue, co-pyrolysis, interaction, thermogravimetric analysis-Fourier transform infared spectroscopy.*

1. Introduction

In China, abundant oil shale (OS) resources are retorted for shale oil production to alleviate the shortage of petroleum [1]. The approach to achieve it is using Fushun-type retorts, thus around 10–30 tons of oil shale semi-coke (SC) per ton of shale oil is left after production [2]. Due to the absence of available techniques, landfill is adopted, which, on the one hand, occupies a lot of land, and, on the other hand, causes a great hazard to the environment [3].

Additionally, China is the world's largest producer and exporter of furfural, one of the most important chemicals. Furfural residue (FR) is the solid waste remaining after extracting furfural from corncob. There is generated about 12–15 tons of FR per ton of furfural production, and millions of tons of it

_____

* Corresponding author: e-mail *tracycqu@163.com*

are discharged annually [4]. At the same time, there is no effective method for FR treatment either and the generated FR is dumped in the field directly, resulting in a serious environmental pollution. Hence, there is an urgent need for a clean and effective method to dispose of SC and FR. The co-utilization technology is deemed to be one alternative to handle solid wastes in an environmentally friendly and highly efficient manner. Semi-coke is high-ash and low-carbon, in contrast, low ash and high carbon feature furfural residue. Thus, it is recommended to deal with SC and FR simultaneously to balance each other's disadvantages. Qin et al. [5] proposed that SC should be burnt with FR in the fluidized bed, and investigated co-combustion characteristics using a thermogravimetric analyzer (TGA). The results indicated that with increasing FR mass fraction, the advance ignition and burnout were achieved and combustion characteristics were improved. Synergy occurred in every stage, and the above processes reciprocally promoted each other vigorously only at the SC/FR mass ratio of 4:6.

Generally, compared with incineration, pyrolysis is recognized as a more potential and attractive technology for converting raw heterogeneous feedstock into various valuable products. Furfural residue is comprised primarily of cellulose, hemicellulose and lignin and can be separated into high-calorific-value by-products using pyrolysis techniques [6]. Literature shows that the metal salts of SC exert a promoting or inhibiting effect on the cracking of hydrocarbons depending on the type of biomass. Hu et al. [7] claimed that the inhibiting effect of SC on the co-pyrolysis of OS with *C. vulgaris* was stronger than their inhibiting effect, while Jiang et al. [8] demonstrated that the addition of SC facilitated the thermal release during the co-pyrolysis of OS with spent mushroom substrate and increased the bio-oil yield.

Up to the present time, studies on the co-pyrolysis of FR and SC have been relatively few, and the mechanism of influence of the latter on FR pyrolysis is still unknown. Furthermore, the development of said process and proper equipment require the understanding of the dominating reaction mechanism, the adoption of optimum pyrolysis parameters as well as the determination of optimum blending ratio [9]. All these factors are important for the subsequent industrial application of the process.

In the present work, the pyrolysis characteristics of SC, FR and their blends with different mass ratios at 20, 30, 40 and 50 °C/min were studied through thermogravimetric analysis (TGA) coupled with Fourier transform infrared spectrometry (FTIR), revealing the pyrolysis behavior of and mutual interaction between the components, as well as the composition of volatile gas products. The activation energy was obtained using the distributed activation energy model (DAEM), Flynn-Wall-Ozawa (FWO) and Kissinger-Akahira-Sunose (KAS) methods. Moreover, the optimum blending ratio of FR to SC was figured out for overall consideration. This paper contributes to filling in the gap in the knowledge of the co-pyrolysis of FR and SC and offers reference to its application in industry.

2. Experimental methods

2.1. Materials

Semi-coke and furfural were separately collected from the Fushun oil shale retorting plant and the Fushun furfural factory located in Liaoning Province, China. Because of its high moisture content, the drying of FR was needed [5]. Table 1 presents the results of ultimate and proximate analyses of samples. The samples were, in accordance with national standards, ground and sieved from 0 to 0.21 mm. Using a rotary mixer with a stirring shaft, FR was blended with SC in a certain proportion as evenly as possible. The samples at the blending ratios of SC/FR of 1:0, 3:1, 1:1, 1:3 and 0:1 were labeled as S_1, S_2, S_3, S_4 and S_5.

Table 1. Ultimate and proximate analyses of SC and FR

Sample	Ultimate analysis, wt%					Proximate analysis, wt%				$Q_{ad,net}$, kJ/kg
	C_{ad}	H_{ad}	O_{ad}	N_{ad}	S_{ad}	M_{ad}	V_{ad}	A_{ad}	FC_{ad}	
SC	6.32	0.78	3.74	0.6	0.45	0.6	7.71	87.51	4.18	2403
FR	48.62	5.16	36.8	0.37	0.78	3.52	68.5	4.75	23.23	17365

2.2. Apparatus and procedure

Pyrolysis experiments were performed using a NETZSCH STA 409PC thermogravimetric analyzer (Germany). About 10 mg samples were spread evenly in an alumina crucible under an inert atmosphere of high-purity nitrogen at a flow rate of 40 ml/min and heated at a rate of 20, 30, 40 and 50 °C/min, respectively, from room temperature to 1100 °C. For the baseline correction, a separate blank run was conducted using an empty pan at each heating rate. The same experiments were repeated at least twice to ensure the reproducibility of experiments and the accuracy of data.

The gaseous products of the pyrolysis of SC, FR and their blends were determined by a Bruker TENSOR 27 FT-IR spectrometer (Germany). Before experiments, nitrogen was passed through the device for 5 min to correct the background baseline. The gaseous products travelled through the transfer line which was heated at 180 °C to prevent the condensation of gases, then the system started to collect the FTIR spectra of gases. The spectra were taken at a wavenumber from 4000 cm^{-1} to 400 cm^{-1} with a resolution of 4 cm^{-1}, and 16 scans per sampling.

3. Results and discussion

3.1. Pyrolysis characteristics of samples

TG and DTG curves of samples at a heating rate of 40 °C/min are displayed in Figures 1a and 1b, respectively. The pyrolysis process of samples could be roughly divided into three stages. In the first stage, a slight mass loss occurred below 150 °C, which was attributed to the loss of free water and interlayer water. As the temperature rose, there was observed an obvious weight loss, corresponding to the devolatilization of FR. The thermal degradation of FR occurred in the temperature range from 200 to 600 °C and consisted of two stages. In the first stage, a sharp mass loss peak appearing at 200–400 °C was ascribed to the decomposition of cellulose, hemicellulose and partial lignin. In the second stage, a mass loss shoulder formed at 400–600 °C was related to the continuous devolatilization of FR with some lignin and char [10]. Besides, the thermal decomposition of SC took place at 450–650 °C, and there was only an unapparent region in its DTG curve. The reason was that in the retorting process of OS, most of organic matter was decomposed, thus the weight loss of SC at this stage was attributed to the degradation of low-molecular-weight residual organic matter. When the temperature was further raised to approximately 700 °C, some minerals underwent thermal decomposition and their TG and DTG curves gradually became smooth [11]. Thus, in general, the pyrolysis process of FR, SC and their blends could be divided into the phases of water evaporation, and decomposition of organic and inorganic matter.

Figure 1 also reveals that all the TG and DTG curves of blends were formed between those of onefold components. The tendency refers to that with increasing FR mass fraction, the total weight loss, pyrolysis range width and maximum weight loss rate increased, showing that FR contained more volatile matter and its pyrolysis behavior was superior to that of SC. This was consistent with proximate analysis results. Hence, it was claimed that the addition of FR improved the pyrolysis performance of blended samples.
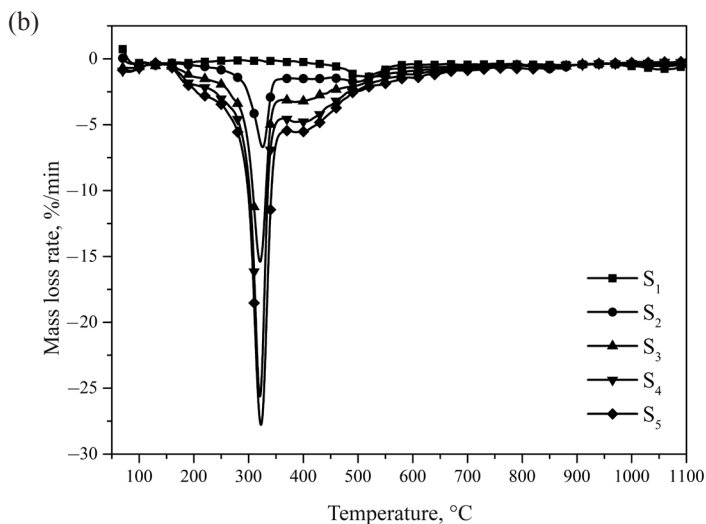
(b)
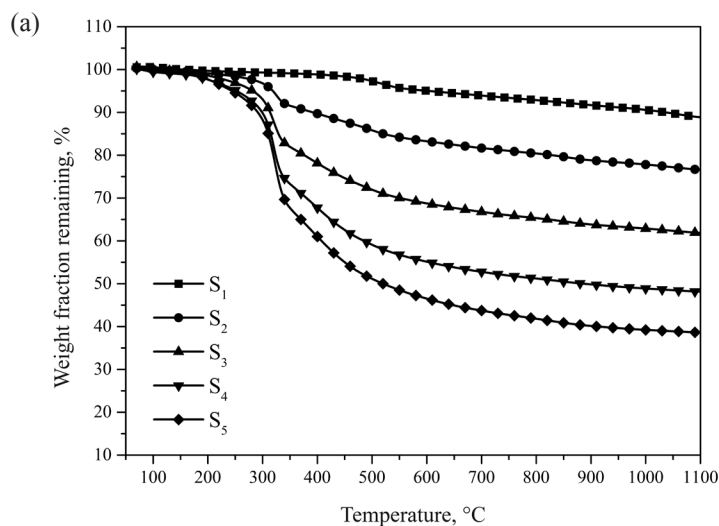
Fig. 1. TG (a) and DTG (b) curves of samples S_1–S_5 at a heating rate of 40 °C/min.

Figure 2 shows the TG and DTG curves of sample S_2 at different heating rates. It can be seen from the figure that with increasing heating rate, the maximum weight loss rate and peak temperature increased and the DTG curve moved toward higher temperature. This could be explained by the shortening of the reaction time with increasing heating rate, which was unfavourable for the pyrolysis process. Also, the temperature and pressure gradient of the exterior and interior of the sample rose, resulting in the increase of heat diffusion resistance, after which the thermal hysteresis occurred. However, the sample underwent a stronger thermal shock at a higher heating rate, which enhanced the intensity of pyrolysis.
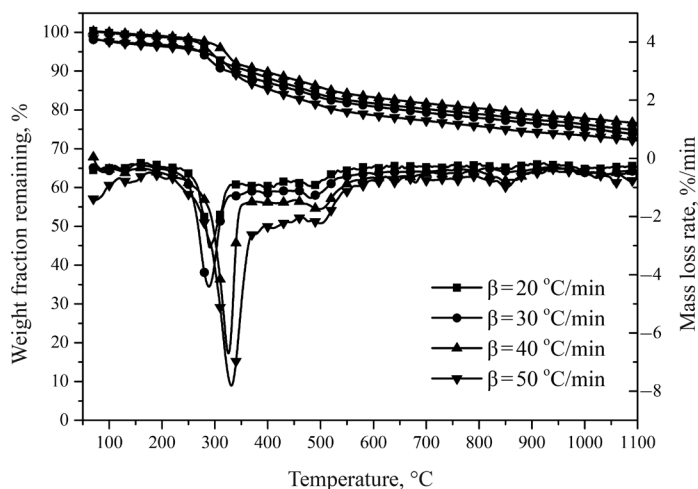

Fig. 2. TG and DTG curves of sample S_2 at different heating rates.

In this work, a pyrolysis index (D) was used to evaluate the pyrolysis characteristics of FR, SC and their blends, as described by Equation (1) [12]:

$$D = \frac{(dw/dt)_{max}\,(dw/dt)_{mean}\,M_{\infty}}{T_i T_{max} \Delta T_{1/2}},$$ (1)

where $(dw/dt)_{max}$ and $(dw/dt)_{mean}$ represent the maximum and average mass loss rate, respectively, M_{∞} is the mass loss, T_i is the initial temperature determined by extrapolating TG-DTG data, T_{max} and $\Delta T_{1/2}$ are the temperature of maximum mass loss rate and peak half-width, respectively. A higher value of D suggested the better pyrolysis release characteristics of the sample.

Table 2 presents the pyrolysis characteristics of samples at a heating rate of 40 °C/min. It is obvious that when the FR mass fraction was increased from 0 to 25%, T_i and T_{max} decreased respectively from 460 to 299 °C and from 524.5 to 325.6 °C, indicating that the pyrolysis process was accelerated by adding FR. Also, with increasing FR mass fraction, D increased from 0.03×10^{-11} min^{-2} °C^{-3} to 128.96×10^{-11} min^{-2} °C^{-3}, demonstrating that the addition of FR improved the pyrolysis characteristics of samples. On the other hand, the experimental values of pyrolysis characteristics of blends did not agree with calculated ones, giving evidence of interactions between SC and FR.

Table 2. The pyrolysis characteristics of samples at a heating rate of 40 °C/min

Sample	T_i, °C	T_{max}, °C	$\Delta T_{1/2}$, °C	$(dw/dt)_{max}$, %/min	$(dw/dt)_{mean}$, %/min	M_{∞}, %	$D \times 10^{11}$, min^{-2} °C^{-3}
S_1	460	524.5	88.2	−1.38	−0.42	11.13	0.03
S_2	299	325.6	33.9	−6.7	−0.88	23.41	4.18
$S_{2,cal}$	417.8	474	74.3	−7.98	−0.89	23.7	1.14
S_3	295	321.1	32.4	−15.4	−1.43	38.12	27.35
$S_{3,cal}$	375.5	423.6	60.3	−14.58	−1.36	36.26	7.5
S_4	292.1	320.8	26.1	−25.62	−1.94	51.83	105.39
$S_{4,cal}$	333.3	373	46.4	−21.18	−1.83	48.83	32.81
S_5	291	322.6	32.4	−27.78	−2.3	61.39	128.96

3.2. Synergy between blended samples

To verify the coupling interactions and explore the underlying mechanism during the co-pyrolysis of SC and FR, the theoretical TG and DTG curves were calculated and the synergy was quantitatively determined by the interaction coefficient (*f*) and the relative error of mean square root (*rms*) [13], as described by Equations (2)–(5):

$$M_{cal} = x_{SC} M_{SC} + x_{FR} M_{FR} , \tag{2}$$

$$\left(\frac{dw}{dt} \right)_{cal} = x_{SC} \left(\frac{dw}{dt} \right)_{SC} + x_{FR} \left(\frac{dw}{dt} \right)_{FR} , \tag{3}$$

$$f = \frac{R_{exp} \Delta T_{1/2,exp} / T_{max,exp}}{R_{cal} \Delta T_{1/2,cal} / T_{max,cal}} , \tag{4}$$

$$rms = \sqrt{\frac{\sum_{i}^{n} \left(\frac{x_{exp}^{i} - x_{cal}^{i}}{x_{cal}^{i}} \right)^2}{n}} , \tag{5}$$

where x is the mass fraction of each individual fuel in the mixture, M and (dw/dt) are respectively the residue mass loss and the mass loss rate of an individual fuel, R is the value of DTG peak point, $\Delta T_{1/2}$ is the peak half-width, x^i is the weight fraction remaining of NO. i, and n is the number of points selected in the experiment.

Figure 3 illustrates the experimental and calculated curves of blends at a heating rate of 40 °C/min. It is clear that the co-pyrolysis of FR and SC is not a simple superposition of these components, but also involves their mutual influences. Table 3 lists the synergy evaluation parameters of the mixture of SC and FR. As mentioned above, synergy behaved differently with the variation of proportions of the blend components. When the SC mass fraction was 25 or 50%, the experimental values of total weight loss and maximum mass loss rate were both higher than calculated ones, and the value of f was larger than 1, suggesting positive interactions between SC and FR. However, the case was opposite with the sample of 75% SC mass fraction, the experimental values of total weight loss and maximum mass loss rate of which were slightly smaller than calculated ones, and the f value was smaller than 1. This implied negative interactions between SC and FR and an undesirable course of the co-pyrolysis process. This might be explained by the presence of minerals such as SiO_2, Al_2O_3, Fe_2O_3 and CaO in SC [14]. Previously it has been demonstrated that the active acid sites in Al_2O_3 could catalyze the decomposition of biomass [8].

Also, alkali and alkaline earth metal elements were able to exert a catalytic effect on the pyrolysis of biomass [15]. Moreover, the presence of SC could enhance the heat transfer among solid particles [16]. Thus, all the above factors combined together accelerated the decomposition of FR. On the other hand, the larger amount of SC particles in the blend might coat the FR powder, thus increasing the absorption effect, as well as the resistance to heat and mass transfer [17]. This hampered the release of volatile matter from FR. Hence, it could be further concluded that the pyrolysis process of FR was delayed by too high a proportion of SC. Considering the above, in order to promote the decomposition of FR and hinder that of SC, the optimal blending ratio of FR and SC was selected to be 1:1.
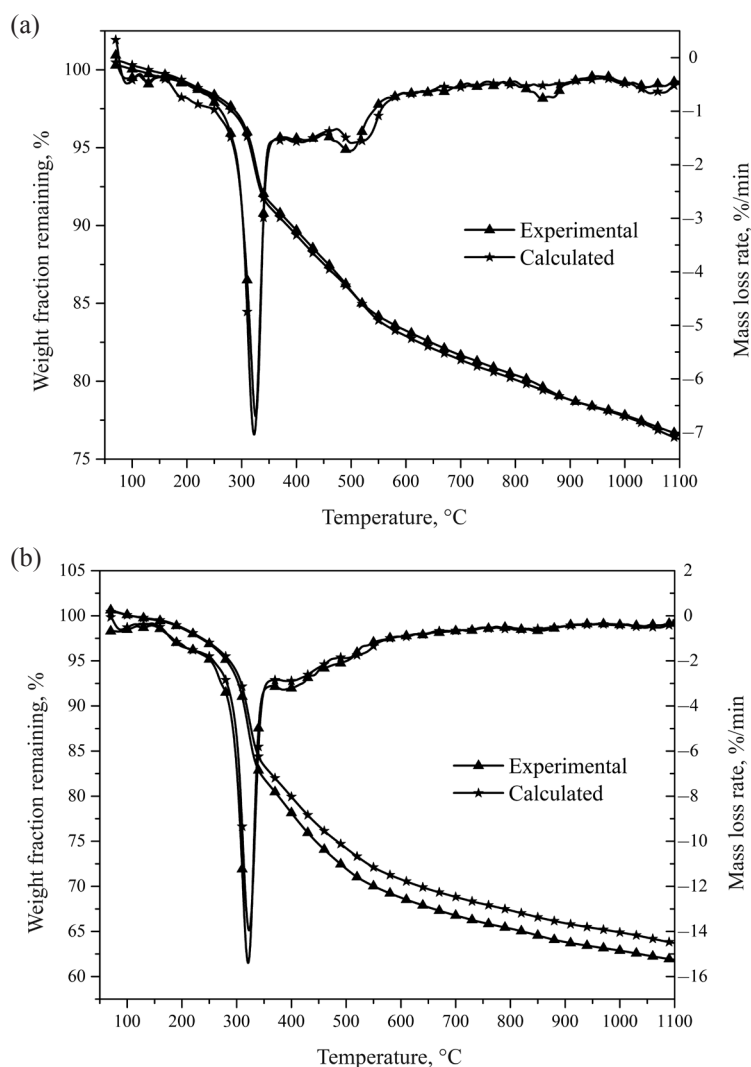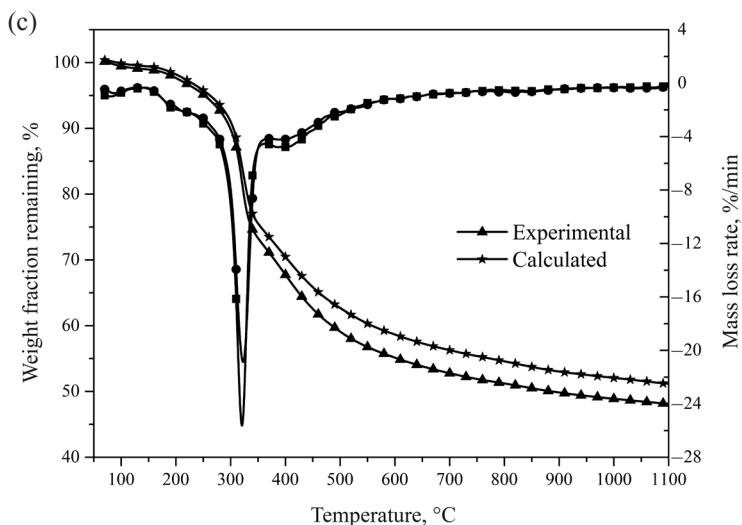
Fig. 3. Comparison between the experimental and calculated curves of samples S_2 (a), S_3 (b) and S_4 (c) at a heating rate of 40 °C/min.

Table 3. Synergy evaluation parameters of blended samples

Sample	*f*	*rms*
S_2	0.97	0.003
S_3	1.11	0.021
S_4	1.21	0.042

3.3. TGA-FTIR of gaseous products

Figure 4 shows the three-dimensional infrared adsorption spectra of sample S_3 at a heating rate of 20 °C/min. S_3 can be seen to contain several gaseous products, such as carbonyl, hydroxyl, carbon dioxide, carbon monoxide, methane, etc. The peaks at 1734 cm^{-1} and 1220 cm^{-1} were attributed to carbonyl and hydroxyl groups, confirming the presence of aldehydes or organic acid, and alcohols or phenols [6]. The breaking of both the methoxy group with lower bond energy and the methylene group with higher bond energy led to the release of CH_4. The bands at 2384 cm^{-1} and 2184 cm^{-1} indicated the formation of CO_2 and CO, respectively, which was generally caused by the cracking of carbonyl [18]. Moreover, the band at 3733 cm^{-1} was assigned to the stretching of the O–H bond, corresponding to the release of H_2O, which was probably produced by the cleavage of aliphatic hydroxyl groups in the side chains of organic polymers [19].
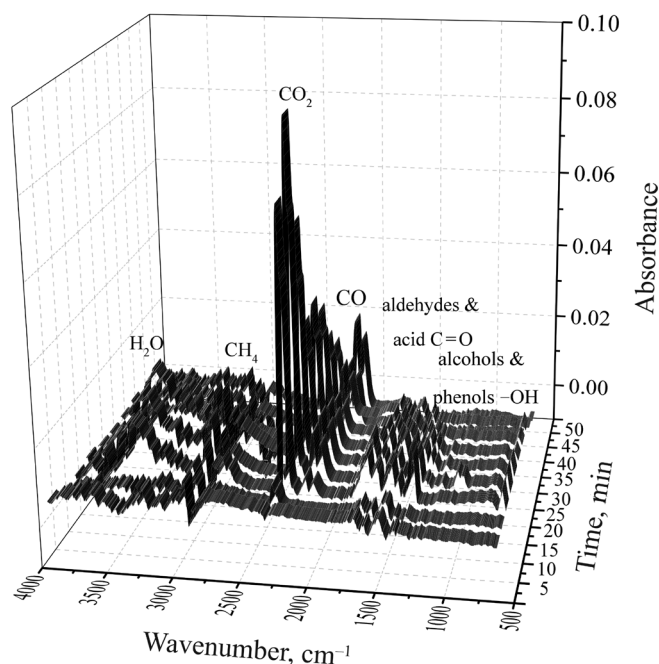
Fig. 4. Three-dimensional infrared absorption spectra in the pyrolysis process of sample S_3.

The Lambert-Beer law suggests that the absorption spectrum at a specific wavenumber linearly depends on gas concentration, and the variation in FTIR peak height reflects the change tendency of gaseous products concentration. Thus, absorbance data at different temperatures can be obtained by fixing the wavenumber to determine the release characteristics of samples, as illustrated in Figure 5. From the figure it can be seen that except CO and CO_2, other gaseous products had one intense absorption peak, while the emission intensity increased before the appearance of the peak in the temperature range of 350–450 °C, decreasing thereafter with rising temperature. The addition of SC facilitated the release of hydroxyl, but slightly inhibited that of CO_2 and CH_4. Besides, it is worthy of note that the rate of release and the total volume of the released compounds were different, yet there was a positive relationship between the release rate of gaseous products and the proportion of FR.
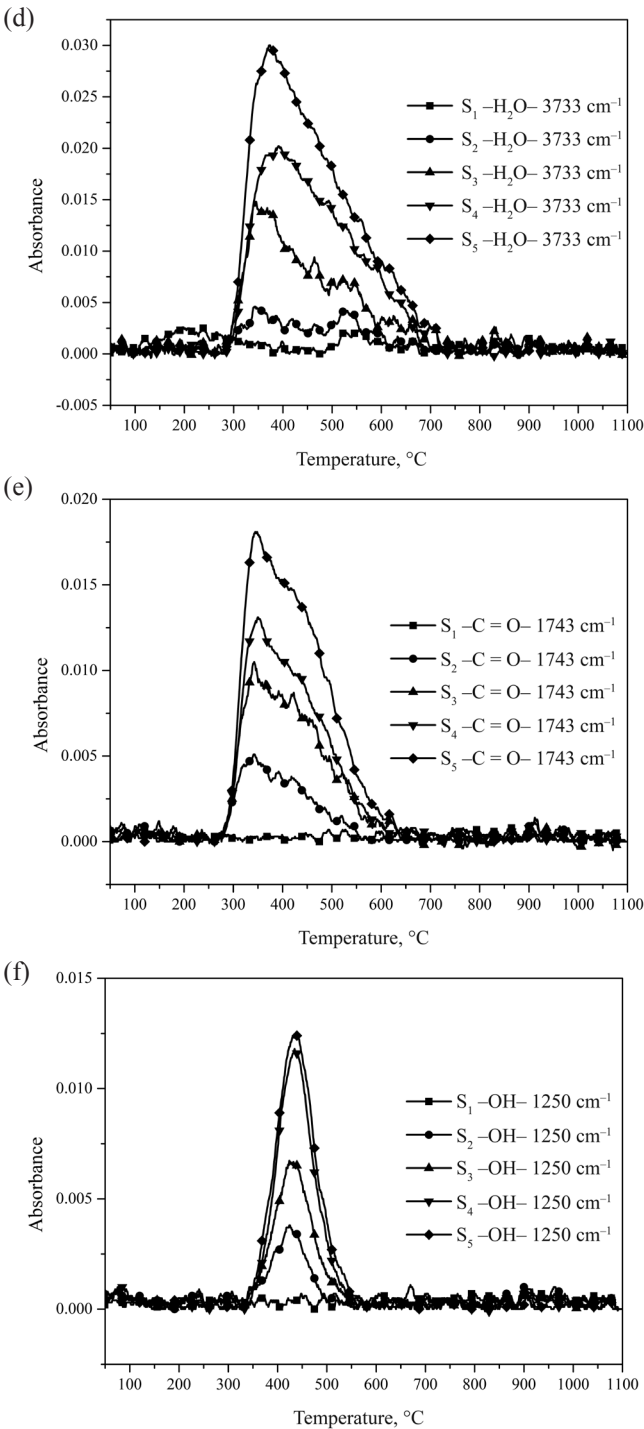
(a)

(b)

(c)

(d)

(e)

(f)
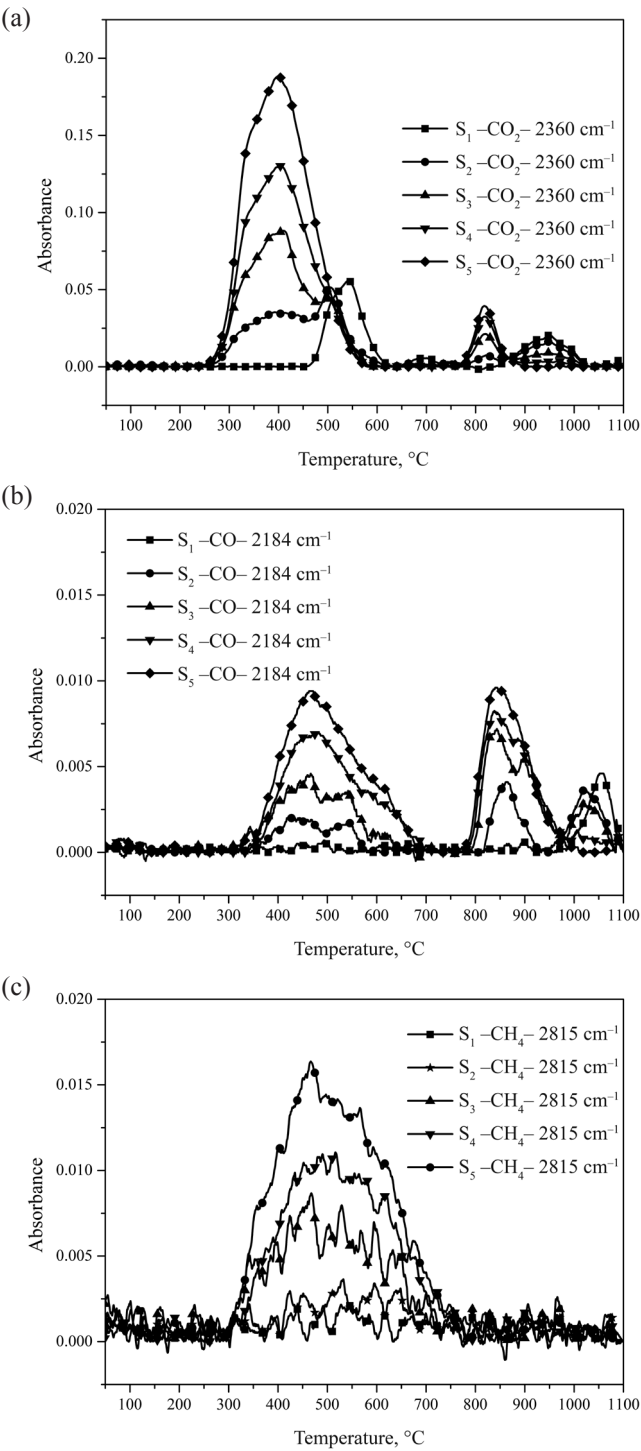
Fig. 5. Gaseous products release rules of samples S_1–S_5.

3.4. Kinetic analysis

In this work, three kinds of model-free methods (DAEM, FWO, KAS) were used to calculate the activation energy, the corresponding equations being as follows [20]:

$$\frac{E}{R} = -\frac{d\ln\beta}{d\left(1/T\right)} - 2T, \tag{6}$$

$$\lg\beta = \lg\left(\frac{AE}{G(\alpha)}\right) - 2.315 - 0.4567\frac{E}{RT}, \tag{7}$$

$$\ln\frac{\beta}{T^2} = \ln\left(\frac{AR}{G(\alpha)E}\right) - \frac{E}{RT}, \tag{8}$$

where α is the conversion degree; β is the heating rate; A, E, R and T are respectively the frequency factor, activation energy, universal gas constant and temperature. Hence, if to plot $\ln\beta$, $\lg\beta$ or $\ln(\beta/T)^2$ vs $1/T$ at selected α, the slope of the curve at different α values is obtained. Then, E values corresponding to α values can be obtained.

The activation energy curves of samples S_2–S_5 at α = 0.1–0.9 in the devolatilization temperature range of 200–600 °C are shown in Figure 6. The correlation coefficients of E were greater than 0.91, implying an acceptable accuracy of the results. The laws governing the change of E established through DAEM, FWO and KAS were similar, and differences in E values among the above methods were smaller than 7 kJ/mol, suggesting that either of them could be used to calculate the pyrolysis kinetics of samples. As seen from Figures 6a–6c, E gradually increased with progressing conversion, indicating the complex nature of the pyrolysis process of a sample. In addition, with increasing SC mass fraction, E increased uniformly, remaining mainly in the range of 50–140 kJ/kg.
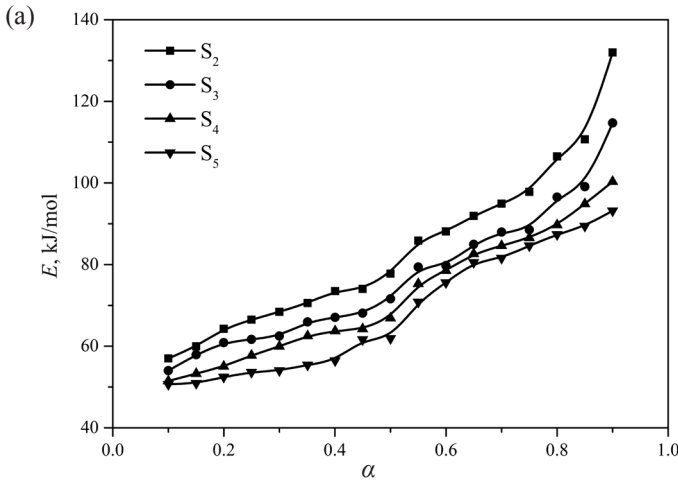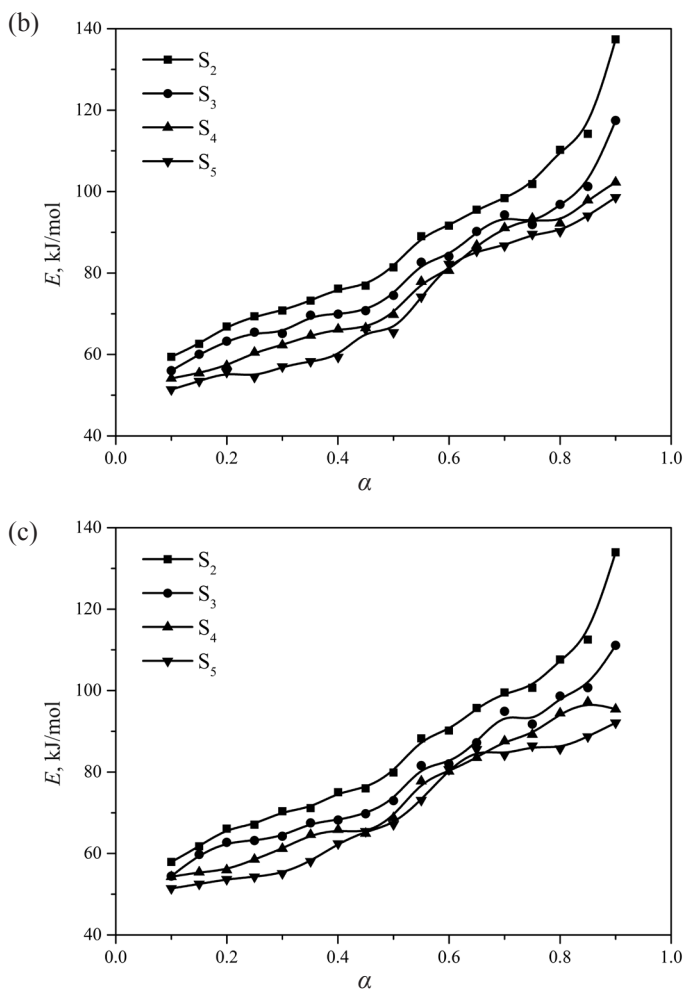
Fig. 6. The relationship between E and α of samples S_2–S_5 by DAEM (a), FWO (b) and KAS (c) methods.

4. Conclusions

The co-pyrolysis characteristics of oil shale semi-coke and furfural residue were studied by thermogravimetric analysis coupled with Fourier transform infrared spectrometry. Some primary results are summarized as follows:

1. The pyrolysis performance of blends improved with increasing furfural residue proportion. The co-pyrolysis of blends was not a simple superposition of individual components, but also involved their mutual influences.

2. Synergy behaved differently with the variation of the mixing ratio. The interaction between the blend components was favourable for co-pyrolysis when the semi-coke mass fraction was 25% or 50%, and unfavorable at said fraction of 75%. Hence, it was recommended to use the semi-coke fraction of 50%.

3. The addition of semi-coke facilitated the release of hydroxyl, but slightly inhibited the release of CO_2 and CH_4.

4. The co-pyrolysis of semi-coke and furfural residue was a multi-process, and its kinetic parameters could be calculated using the distributed activation energy model, Flynn-Wall-Ozawa and Kissinger-Akahira-Sunose methods.

In summary, the industrial application of co-pyrolysis of oil shale semi-coke and furfural residue may have a good prospect, while at a certain mixing ratio semi-coke can act as a catalyst for the pyrolysis of furfural residue.

Acknowledgments

REFERENCES

1. Jiang, X. M., Han, X. X., Cui, Z. G. New technology for the comprehensive utilization of Chinese oil shale resources. *Energy*, 2007, **32**(5), 772–777.
2. Jiang, X. M., Han, X. X., Cui, Z. G. Progress and recent utilization trends in combustion of Chinese oil shale. *Prog. Energy Combust. Sci.*, 2007, **33**(6), 552–579.
3. Pae, T., Luud, A., Sepp, M. Artificial mountains in North-East Estonia: Monumental dumps of ash and semi-coke. *Oil Shale*, 2005, **22**(3), 333–343.
4. Wang, Y., Xu, Z. Y., Song, X., Yang, B., Zhang, D. The preparation of low-cost adsorbent for heavy metal based on furfural residue. *Mater. Manuf. Process.*, 2017, **32**(1), 87–92.
5. Qin, H., Wang, W., Liu, H. P., Zhang, L. D., Wang, Q., Shi, C. Y., Yao, K. W. Thermal behavior research for co-combustion of furfural residue and oil shale semi-coke. *Appl. Therm. Eng.*, 2017, **120**, 19–25.
6. Quan, C., Ma, Z. Z., Gao, N. B., He, C. Pyrolysis and combustion characteristics of corncob hydrolysis residue. *J. Anal. Appl. Pyrolysis*, 2018, **130**, 72–78.
7. Hu, Z. F., Ma, X. Q., Li, L. J. The synergistic effect of co-pyrolysis of oil shale

and microalgae to produce syngas. *J. Energy Inst.*, 2016, **89**(3), 447–455.

8. Jiang, H. F., Zhang, M. Y., Chen, J., Li, S., Shao, Y. F., Yang, J. Q., Li, J. F. Characteristics of bio-oil produced by the pyrolysis of mixed oil shale semi-coke and spent mushroom substrate. *Fuel*, 2017, **200**, 218–224.

9. He, Y., Ma, X. Q. Comparative investigation on non-isothermal kinetics for thermo-degradation of lignocellulosic substrate and its chlorinated derivative in atmospheres with CO_2 participation. *Bioresour. Technol.*, 2015, **189**, 71–80.

10. Zhang, X. S., Lei, H. W., Zhu, L., Qian, M., Yadavalli, G., Wu, J., Chen, S. L. Thermal behavior and kinetic study for catalytic co-pyrolysis of biomass with plastics. *Bioresour. Technol.*, 2016, **220**, 233–238.

11. Williams, P. T., Ahmad, N. Investigation of oil-shale pyrolysis processing conditions using thermogravimetric analysis. *Appl. Energy*, 2000, **66**(2), 113–133.

12. Fang, S. W., Yu, Z. S., Lin, Y. S., Hu, S. C., Liao, Y. F., Ma, X. Q. Thermo-gravimetric analysis of the co-pyrolysis of paper sludge and municipal solid waste. *Energy Convers. Manag.*, 2015, **101**, 626–631.

13. Qin, H., Yue, Y. K., Zhang, L., Liu, Y. Y., Chi, M. S., Liu, H. P., Wang, Q., Liu, B. Study on co-combustion kinetics of oil shale sludge and semi-coke. *Energy Fuels*, 2016, **30**(3), 2373–2384.

14. Yang, Y., Lu, X. F., Wang, Q. H., Mei, L., Song, D. C., Hong, Y. Experimental study on combustion of low calorific oil shale semicoke in fluidized bed system. *Energy Fuels*, 2016, **30**(11), 9882–9890.

15. Nguyen, T. S., Zabeti, M., Lefferts, L., Brem, G., Seshan, K. Conversion of lignocellulosic biomass to green fuel oil over sodium based catalysts. *Bioresour. Technol.*, 2013, **142**, 353–360.

16. Niu, M. T., Wang, S., Han, X. X., Jiang, X. M. Yield and characteristics of shale oil from the retorting of oil shale and fine oil-shale ash mixtures. *Appl. Energy*, 2013, **111**, 234–239.

17. Grierson, S., Strezov, V., Ellem, G., Mcgregor, R., Herbertson, J. Thermal characterisation of microalgae under slow pyrolysis conditions. *J. Anal. Appl. Pyrolysis*, 2009, **85**(1–2), 118–123.

18. Qin, L. B., Han, J., He, X., Zhan, Y. Q., Yu, F. Recovery of energy and iron from oily sludge pyrolysis in a fluidized bed reactor. *J. Environ. Manage.*, 2015, **154**, 177–182.

19. Meng, A. H., Zhou, H., Qin, L., Zhang, Y. G., Li, Q. H. Quantitative and kinetic TG-FTIR investigation on three kinds of biomass pyrolysis. *J. Anal. Appl. Pyrolysis*, 2013, **104**, 28–37.

20. Yang, Y., Lu, X. F., Wang, Q. H. Investigation on the co-combustion of low calorific oil shale and its semi-coke by using thermogravimetric analysis. *Energy Convers. Manag.*, 2017, **136**, 99–107.